COMMUNICATIONS IN COMPUTATIONAL PHYSICS
Vol. **1**, No. 1, pp. 1-21

Commun. Comput. Phys.
February 2006

A Fourth-Order Upwinding Embedded Boundary Method (UEBM) for Maxwell's Equations in Media with Material Interfaces: Part I

Shaozhong Deng[1] and Wei Cai[1,*]

[1] *Department of Mathematics and Statistics, University of North Carolina at Charlotte, Charlotte, NC 28223-0001, USA.*

Abstract. In this paper, we present a new fourth-order upwinding embedded boundary method (UEBM) over Cartesian grids, originally proposed in the *Journal of Computational Physics (190, pp. 159, 2003)* as a second-order method for treating material interfaces for Maxwell's equations. In addition to the idea of the UEBM to evolve solutions at interfaces, we utilize the ghost fluid method to construct finite difference approximation of spatial derivatives at Cartesian grid points near the material interfaces. As a result, Runge-Kutta type time discretization can be used for the semi-discretized system to yield an overall fourth-order method, in contrast to the original second-order UEBM based on a Lax-Wendroff type difference. The final scheme allows time step sizes independent of the interface locations. Numerical examples are given to demonstrate the fourth-order accuracy as well as the stability of the method. We tested the scheme for several wave problems with various material interface locations, including electromagnetic scattering of a plane wave incident on a planar boundary and a two-dimensional electromagnetic application with an interface parallel to the y-axis.

1 Introduction

The finite difference time domain (FDTD) Yee scheme, first introduced by Yee in 1966 [1] and later developed by Taflove and others [2], has been used for a broad range of application problems in computational electromagnetics. The staggered Yee scheme has been demonstrated to be robust, efficient, and simple to implement. However, when used to model curved objects or to solve Maxwell's equations in media with material interfaces, the Yee scheme requires locally conforming meshes for the irregular boundaries or the material interfaces. Otherwise, it will reduce to at best first-order accuracy and may produce locally non-convergent results [3, 4]. Furthermore, for Maxwell's equations with discontinuous coefficients, the Yee scheme might not be able to capture the possible discontinuity of the solution across the interfaces.

*Correspondence to: Department of Mathematics and Statistics, University of North Carolina at Charlotte, Charlotte, NC 28223-0001, USA. Email: wcai@uncc.edu

A number of finite difference methods have been proposed in the past for modeling time-domain Maxwell's equations with curved material interfaces. The usual and straightforward approach is to introduce appropriate local modifications into the Yee scheme but still keep the staggered grid [4, 5]. Recently, there are some studies of high-order embedded FDTD schemes for time-domain Maxwell's equations with material interfaces, including the non-dissipative staggered fourth-order accurate explicit method and the staggered fourth-order compact implicit method by Yefet et al [6, 7], and the explicit fourth-order staggered method and the explicit fourth-order orthogonal curvilinear staggered grid method by Xie et al [8, 9]. Also, high-order FDTD methods via hierarchical implicit derivative matching are presented in [10].

In this paper, we present a new fourth-order upwinding embedded boundary method (UEBM) over Cartesian grids, originally proposed in [11] as a second-order method for treating material interfaces for Maxwell's equations. In addition to the idea of the UEBM to evolve solutions at the interfaces, we utilize the ghost fluid method to construct finite difference approximation of spatial derivatives at Cartesian grid points near the material interfaces. As a result, Runge-Kutta type time discretization can be used for the semi-discretized system to yield an overall fourth-order method, in contrast to the original second-order method based on a Lax-Wendroff type difference. The fourth-order method still uses a simple Cartesian grid and a central difference scheme for mesh points away from the interfaces. Solutions at both sides of the interfaces are calculated with an upwinding strategy while preserving the possible physical jump conditions. Previous numerical methods making use of Cartesian grids for the approximation of one-dimensional hyperbolic equations could also be found in [12]-[14].

The ghost fluid method (GFM) was originally designed to treat contact discontinuities in the inviscid Euler equations in [15], and since then it has been generalized to handle irregular boundaries in a variety of problems [16]-[28]. For examples, with the use of the so-called ghost cells (based on the GFM), Gibou et al proposed in [20] a second-order accurate finite difference method for Poisson equations, and most recently in [21] a fourth-order accurate finite difference discretization for the Laplace and heat equations on irregular domains with Dirichlet boundary conditions on the irregular interfaces. For second-order wave equations, by using ghost points on either side of the interfaces, Kreiss et al proposed several second-order embedded boundary methods with Dirichlet boundary condition [25, 26], Neumann boundary condition [27], and jump conditions [28] on the irregular interfaces, respectively.

In this paper, we shall combine the GFM with the UEBM to derive high-order Cartesian grid based finite difference methods for hyperbolic systems. In particular, we shall utilize the ideas in [21] to develop a fourth-order accurate finite difference method for one-dimensional time-domain Maxwell's equations with discontinuous coefficients. First, the equations are discretized in space on a uniform Cartesian grid and the interface is allowed to locate between Cartesian grid points in an arbitrary fashion. Then, ghost points are introduced in the neighborhood of the interface, and used in the discretization of the spatial derivatives in the wave equations. To capture the boundary conditions across the interface, like in the original UEBM, the solutions at both sides of the interface are calculated by one-sided extrapolations of the solutions from the corresponding sides of the interface. Since in a hyperbolic system, the upwind characteristic information should be unaffected by the material interface, the two interface solutions are so

constructed such that both the jump condition and the upwinding characteristic properties are observed.

The rest of the paper is organized as follows. In Section 2, we introduce the new fourth-order UEBM for scalar wave equations while its extension to one-dimensional system is given in Section 3. In Section 4, we present a series of numerical examples to show the fourth-order accuracy and the stability for time marching step sizes independent of the interface locations. Finally, a conclusion is given in Section 5.

2 One-dimensional scalar wave equation

To demonstrate the basic idea of the fourth-order UEBM, we begin by considering the following scalar wave equation

$$\frac{\partial u}{\partial t} + c\,\frac{\partial u}{\partial x} = 0, \qquad x \in \Omega = [a,b], \tag{2.1}$$

where the wave speed c is assumed to be positive and discontinuous at $x_d \in (a,b)$, i.e.,

$$c = \begin{cases} c^- > 0, & x < x_d, \\ c^+ > 0, & x > x_d. \end{cases}$$

The solution $u(x,t)$ is in general discontinuous at the interface x_d, and is assumed to satisfy the following given interface jump condition

$$r^+ u(x_d^+, t) - r^- u(x_d^-, t) = g(t), \tag{2.2}$$

where $u(x_d^-, t)$ and $u(x_d^+, t)$ represent the two one-sided limits of the solution as x approaches the interface x_d.

We shall employ a semi-discrete approach to develop a fourth-order finite difference method for (2.1). The spatial computational domain $[a,b]$ is discretized into cells of size Δx to form a uniform Cartesian grid $\{x_i = a + i\Delta x,\ 0 \le i \le N,\ \Delta x = (b-a)/N\}$. Let U_i^n denote the numerical approximation of the solution $u(x_i, t_n)$, and also let $U^{-,n}$ and $U^{+,n}$ denote the numerical approximation of the solutions $u(x_d^-, t_n)$ and $u(x_d^+, t_n)$, respectively.

2.1 Approximation of spatial derivative at Cartesian grids

For a semi-discrete approach, let us first focus on the discretization of the spatial derivative u_x. To compute a fourth-order accurate approximation of u_x at the node x_i, we use

$$(u_x)_i \approx \frac{1}{12\Delta x}\left(U_{i-2} - 8U_{i-1} + 8U_{i+1} - U_{i+2}\right). \tag{2.3}$$

However, the discretization (2.3) is valid only if all the nodes in the fourth-order stencil belong to the same side of the interface, and needs to be modified otherwise. Suppose that the discontinuity, x_d, lies between the nodes x_j and x_{j+1}, and $x_d = x_j + \theta\Delta x$ (see Fig. 1), where $0 \le \theta < 1$ is the cell fraction. We seek to approximate u_x at the nodes x_{j-1} and x_j. Since the

solution might not be continuous across the interface, we need valid values for U_{j+1} and U_{j+2} that "emulate" the behavior of the solution to the left of the interface. As discussed in [21], this can be achieved by introducing ghost cells near the discontinuity, or in another word, ghost values U^G_{j+1} and U^G_{j+2} to the right of the interface defined by extrapolation of the solution to the left of the interface. Then, the spatial discretization (2.3) for the irregular grid points x_{j-1} and x_j can be rewritten as

$$(u_x)_{j-1} \approx \frac{1}{12\Delta x}\left(U_{j-3} - 8U_{j-2} + 8U_j - U^G_{j+1}\right), \tag{2.4}$$

$$(u_x)_j \approx \frac{1}{12\Delta x}\left(U_{j-2} - 8U_{j-1} + 8U^G_{j+1} - U^G_{j+2}\right). \tag{2.5}$$

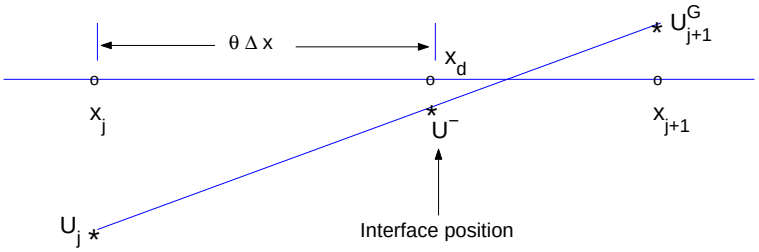

Figure 1: Illustration of the ghost cell and the ghost value (with linear extrapolation).

We could construct a cubic extrapolant $L(x)$ of $u(x)$ to the left of the interface, such that $L(-2\Delta x) = U_{j-2}, L(-\Delta x) = U_{j-1}, L(0) = U_j$ and $L(\theta\Delta x) = U^-$. Then the ghost values at the nodes x_{j+1} and x_{j+2} are defined as $U^G_{j+1} = L(\Delta x)$ and $U^G_{j+2} = L(2\Delta x)$, respectively. In practice, however, when the cell fraction θ is small, we instead construct a cubic extrapolant $L(x)$ such that $L(-2\Delta x) = U_{j-3}, L(-\Delta x) = U_{j-2}, L(0) = U_{j-1}$, and $L((1+\theta)\Delta x) = U^-$. Note that in this case, we use U^- rather than U_j in the extrapolation, and it is for this reason that, in addition to the solution at all grid points, at each time step we need to calculate the solution at both sides of the interface as well. Accordingly, the ghost values at the nodes x_{j+1} and x_{j+2} are defined as $U^G_{j+1} = L(2\Delta x)$ and $U^G_{j+2} = L(3\Delta x)$, respectively. We have

$$U^G_{j+1} = L(2\Delta x) = a_1(\theta)U_{j-3} + a_2(\theta)U_{j-2} + a_3(\theta)U_{j-1} + a_4(\theta)U^-, \tag{2.6}$$

$$U^G_{j+2} = L(3\Delta x) = b_1(\theta)U_{j-3} + b_2(\theta)U_{j-2} + b_3(\theta)U_{j-1} + b_4(\theta)U^-, \tag{2.7}$$

where

$$a_1(\theta) = \frac{3(\theta-1)}{3+\theta},\ a_2(\theta) = \frac{8(1-\theta)}{2+\theta},\ \ a_3(\theta) = \frac{6(\theta-1)}{1+\theta},\ \ a_4(\theta) = \frac{24}{F(\theta)},$$

$$b_1(\theta) = \frac{6(\theta-2)}{3+\theta},\ b_2(\theta) = \frac{15(2-\theta)}{2+\theta},\ b_3(\theta) = \frac{10(\theta-2)}{1+\theta},\ b_4(\theta) = \frac{60}{F(\theta)},$$

and $F(\theta) = \prod_{i=1}^{3}(i+\theta)$.

Similarly, to approximate the spatial derivative at the nodes x_{j+1} and x_{j+2}, we require ghost values at the nodes x_{j-1} and x_j, denoted by U^G_{j-1} and U^G_j, respectively, which can "emulate" the behavior of the solution defined to the right of the interface as if no interface is present. Accordingly, the numerical discretization (2.3) of the spatial derivative u_x at the nodes x_{j+1} and x_{j+2} in terms of the ghost values would be

$$(u_x)_{j+1} \approx \frac{1}{12\Delta x}\left(U^G_{j-1} - 8U^G_j + 8U_{j+2} - U_{j+3}\right), \tag{2.8}$$

$$(u_x)_{j+2} \approx \frac{1}{12\Delta x}\left(U^G_j - 8U_{j+1} + 8U_{j+3} - U_{j+4}\right). \tag{2.9}$$

Here, the ghost values U^G_{j-1} and U^G_j could be obtained by a cubic extrapolant $R(x)$ such that $R(0) = U_{j+1}, R(\Delta x) = U_{j+2}, R(2\Delta x) = U_{j+3}$, and $R((\theta-1)\Delta x) = U^+$. Then, the ghost values at the nodes x_{j-1} and x_j are defined as $U^G_{j-1} = R(-2\Delta x)$ and $U^G_j = R(-\Delta x)$, respectively. But again considering that the cell fraction θ could be very close to one in practice, we use the cubic extrapolant with the conditions that $R(0) = U_{j+2}, R(\Delta x) = U_{j+3}, R(2\Delta x) = U_{j+4}$, and $R((\theta-2)\Delta x) = U^+$, giving the following ghost values at the nodes x_{j-1} and x_j instead

$$U^G_j = R(-2\Delta x) = a_1(1-\theta)U_{j+4} + a_2(1-\theta)U_{j+3} + a_3(1-\theta)U_{j+2} + a_4(1-\theta)U^+, \tag{2.10}$$

$$U^G_{j-1} = R(-3\Delta x) = b_1(1-\theta)U_{j+4} + b_2(1-\theta)U_{j+3} + b_3(1-\theta)U_{j+2} + b_4(1-\theta)U^+. \tag{2.11}$$

2.2 Calculation of solutions at interface, U^- and U^+

As mentioned earlier, to capture the boundary conditions across the material interfaces using a Cartesian grid, we need to keep track of the solution at both sides of the interfaces as well. Please note that they are also required in calculating the ghost values for points in the neighborhood of the interfaces. Since the solution of Eq. (2.1) represents a wave propagating from the left to the right, we calculate U^- by a cubic extrapolant $P(x)$ such that $P(-3\Delta x) = U_{j-3}, P(-2\Delta x) = U_{j-2}, P(-\Delta x) = U_{j-1}$, and $P(0) = U_j$, i.e.,

$$U^- = P(\theta\Delta x) = -\frac{Q(\theta)}{6(\theta+3)}U_{j-3} + \frac{Q(\theta)}{2(\theta+2)}U_{j-2} - \frac{Q(\theta)}{2(\theta+1)}U_{j-1} + \frac{Q(\theta)}{6\theta}U_j, \tag{2.12}$$

where $Q(\theta) = \prod_{i=0}^{3}(i+\theta)$ (when $\theta = 0, U^- = U_j$), and then calculate U^+ simply using the jump condition (2.2),

$$U^+ = \frac{1}{r^+}\,(g + r^- U^-). \tag{2.13}$$

Remark 1: The above fourth-order central finite difference scheme, together with its local modification in the neighborhood of the interface, can be applied at all nodes in a bounded domain except at x_0, x_1, x_{N-1} and x_N. Since the solution of Eq. (2.1) represents a wave propagating from the left to the right, a physical boundary condition shall be imposed at the first node

x_0. At the other three nodes, the following third-order accurate one-sided approximations are employed as numerical boundary conditions in order to globally approximate the derivative.

$$(u_x)_1 \approx \frac{1}{6\Delta x}\left(-2U_0 - 3U_1 + 6U_2 - U_3\right), \tag{2.14}$$

$$(u_x)_{N-1} \approx \frac{1}{6\Delta x}\left(U_{N-3} - 6U_{N-2} + 3U_{N-1} + 2U_N\right), \tag{2.15}$$

$$(u_x)_N \approx \frac{1}{6\Delta x}\left(-2U_{N-3} + 9U_{N-2} - 18U_{N-1} + 11U_N\right). \tag{2.16}$$

Remark 2 (Avoiding downwind differencing near material interfaces): When the cell fraction $\theta = 0$, the approximations (2.4) and (2.5) will reduce to one-sided approximations like (2.15) and (2.16), which are stable upwind schemes for the problem being concerned. When the cell fraction $\theta = 1$ (in this case, $U^+ = U_{j+1}$), however, the approximations (2.8) and (2.9) will reduce to the following one-sided approximations

$$(u_x)_{j+1} \approx \frac{1}{6\Delta x}\left(-11U_{j+1} + 18U_{j+2} - 9U_{j+3} + 2U_{j+4}\right), \tag{2.17}$$

$$(u_x)_{j+2} \approx \frac{1}{6\Delta x}\left(-2U_{j+1} - 3U_{j+2} + 6U_{j+3} - U_{j+4}\right). \tag{2.18}$$

Note that the scheme (2.17) is essentially an unstable downwind scheme (as confirmed by our numerical tests). For this reason, when θ is close to one, instead of using (2.8), we calculate U_{j+1} by constructing a cubic interpolant $S(x)$ such that $S(\Delta x) = U_{j+2}, S(2\Delta x) = U_{j+3}, S(3\Delta x) = U_{j+4}$, and $S((\theta - 1)\Delta x) = U^+$. Then, we have

$$U_{j+1} = S(0) = \frac{-6}{T(\theta)}U^+ + \frac{3(1-\theta)}{2-\theta}U_{j+2} - \frac{3(1-\theta)}{3-\theta}U_{j+3} + \frac{1-\theta}{4-\theta}U_{j+4}, \tag{2.19}$$

where $T(\theta) = \prod_{i=2}^{4}(\theta - i)$.

Remark 3: It has been theoretically shown and numerically demonstrated that, when a certain order finite difference method is used to approximate mixed initial boundary value problems, the use of a local one-order-lower scheme at a finite number of grid points will not affect the global accuracy of the scheme [4] [8][21][29, 30]. For example, when the GFM is used in solving Laplace and heat equations on arbitrary domains, first-, second-, third- and fourth-order accuracy in L_∞ norm is maintained in the case of constant, linear, quadratic and cubic extrapolations, respectively [21]. It is for this reason that we use the cubic extrapolations (2.6)-(2.7) and (2.10)-(2.11) to define ghost values, the cubic extrapolation (2.12) to calculate the interface solution U^-, the cubic interpolation (2.19) to find U_{j+1}, and the one-sided third-order finite difference schemes (2.14)-(2.16) at and near the boundaries as the numerical boundary conditions. As confirmed by numerical experiments in Section 4, the overall fourth-order convergence rate of the fourth-order scheme is maintained.

To have the fourth-order accuracy in both space and time, we use a fourth-order Runge-Kutta scheme for temporal integration as it can provide a relatively large stability region. Specifically, we use the classical four-stage Runge-Kutta scheme even though a further improvement can be achieved by using the high resolution fourth-order low-dissipation and low-dispersion Runge-Kutta scheme proposed by Hu et al [31].

3 One-dimensional wave system

The discretization scheme discussed in Section 2 for scalar wave equations can be extended naturally to the following system of linear wave equations

$$\frac{\partial \mathbf{u}}{\partial t} + A\frac{\partial \mathbf{u}}{\partial x} = 0, \qquad x \in \Omega = [a,b], \tag{3.1}$$

where $\mathbf{u}(x,t) = (u_1(x,t), \cdots, u_n(x,t))^T$. The coefficient matrix A has different formulas across the discontinuity $x_d \in (a,b)$ representing a material interface

$$A = \begin{cases} A^-, & x < x_d, \\ A^+, & x > x_d, \end{cases}$$

and, in general, the solution $\mathbf{u}(x,t)$ will be discontinuous across the interface, and its values at the left and the right sides of the interface, $\mathbf{u}(x_d^-,t)$ and $\mathbf{u}(x_d^+,t)$, are assumed to be coupled by the following jump condition

$$R^+\mathbf{u}(x_d^+,t) - R^-\mathbf{u}(x_d^-,t) = \mathbf{g}(t). \tag{3.2}$$

We seek to develop a uniformly fourth-order finite difference method by a semi-discrete approach. For regular grid points, the standard fourth-order central finite difference approximation (2.3) is employed for the spatial discretization

$$(\mathbf{u}_x)_i \approx \frac{1}{12\Delta x}\left(\mathbf{U}_{i-2} - 8\mathbf{U}_{i-1} + 8\mathbf{U}_{i+1} - \mathbf{U}_{i+2}\right). \tag{3.3}$$

At nodes in the neighborhood of the interface, i.e., x_{j-1}, x_j, x_{j+1}, and x_{j+2}, ghost values $\mathbf{U}_{j-1}^G, \mathbf{U}_j^G, \mathbf{U}_{j+1}^G$, and $\mathbf{U}_{j+2}^G$ are defined and used to approximate $\mathbf{u}_x$ in the exactly same fashion as discussed in Section 2 for the case of scalar wave equations.

In general, the coefficient matrix could have eigenvalues of opposite signs, indicating that waves could propagate through the interface in opposite directions. In this case, cubic extrapolations similar to (2.12) are then employed to calculate both $\mathbf{U}^-$ and $\mathbf{U}^+$, the solutions at both sides of the interface. In a hyperbolic problem, however, upwinding components of waves should pass through an interface unaffected by downwind contributions, which implies that for the solutions at both sides of the interface, the upwinding property should be maintained. For the numerical solution to satisfy this upwinding property as well as the jump condition (3.2), special treatment has to be introduced. Suppose that the coefficient matrix A can be diagonalized as follows

$$A = P\Lambda P^{-1},$$

where $\Lambda = \text{diag}(\lambda_1, \lambda_2, \cdots, \lambda_n)$ in which λ_i's are the eigenvalues. Without loss of generality, we assume that $\lambda_1, \cdots, \lambda_p \geq 0$, and $\lambda_{p+1}, \cdots, \lambda_n < 0$. Also for a well-defined hyperbolic problem, A^- and A^+ are assumed to have the same number of positive eigenvalues as well as the same number of negative ones. Then, by introducing the characteristic variable $\mathbf{w} = (w_1, w_2, \cdots, w_n)^T = P^{-1}\mathbf{u}$, first we can rewrite the jump condition (3.2) as

$$Q^+\mathbf{w}^+ - Q^-\mathbf{w}^- = \mathbf{g}, \tag{3.4}$$

where $Q^- = R^-P^-$, $Q^+ = R^+P^+$, and $\mathbf{w}^- = (P^-)^{-1}\mathbf{u}^-$ and $\mathbf{w}^+ = (P^+)^{-1}\mathbf{u}^+$ are the approximations of the characteristic variable $\mathbf{w}$ at the two sides of the discontinuity, respectively. Then we let

$$\mathbf{w}^- = \begin{pmatrix} \mathbf{w}_1^- \\ \mathbf{w}_2^- \end{pmatrix}, \quad \mathbf{w}^+ = \begin{pmatrix} \mathbf{w}_1^+ \\ \mathbf{w}_2^+ \end{pmatrix}$$

be the partitions of $\mathbf{w}^-$ and $\mathbf{w}^+$ based on the signs of the eigenvalues of the coefficient matrix, i.e., $\mathbf{w}_1 = (w_1, \cdots, w_p)^T$ and $\mathbf{w}_2 = (w_{p+1}, \cdots, w_n)^T$, and

$$Q^- = \begin{pmatrix} Q_{11}^- & Q_{12}^- \\ \\ Q_{21}^- & Q_{22}^- \end{pmatrix}, \quad Q^+ = \begin{pmatrix} Q_{11}^+ & Q_{12}^+ \\ \\ Q_{21}^+ & Q_{22}^+ \end{pmatrix} \tag{3.5}$$

be the corresponding partitions of the matrices Q^- and Q^+, respectively. By the upwinding principle, the $\mathbf{w}_1^-$ component of $\mathbf{w}^-$ and the $\mathbf{w}_2^+$ component of $\mathbf{w}^+$ should not be affected by the embedded interface boundary. On the other hand, the $\mathbf{w}_1^+$ component of $\mathbf{w}^+$ and the $\mathbf{w}_2^-$ component of $\mathbf{w}^-$ shall be corrected in an upwinding manner, which can be done by rearranging the jump condition (3.4) as

$$\begin{pmatrix} Q_{11}^+ & -Q_{12}^- \\ Q_{21}^+ & -Q_{22}^- \end{pmatrix} \begin{pmatrix} \mathbf{w}_1^+ \\ \mathbf{w}_2^- \end{pmatrix} = \mathbf{g} - \begin{pmatrix} -Q_{11}^- & Q_{12}^+ \\ -Q_{21}^- & Q_{22}^+ \end{pmatrix} \begin{pmatrix} \mathbf{w}_1^- \\ \mathbf{w}_2^+ \end{pmatrix}. \tag{3.6}$$

Here, the coefficient matrix on the left side of Eq. (3.6) will be invertible for well-posed hyperbolic systems. Once we have the updated characteristic components $\mathbf{w}_1^+$ and $\mathbf{w}_2^-$, the solutions at the interface are calculated by $\mathbf{u}^- = P^-\mathbf{w}^-$ and $\mathbf{u}^+ = P^+\mathbf{w}^+$.

As discussed in Section 2, in the case that the cell fraction θ is very close to zero or one, for the stability concern the corresponding downwind characteristic information in $\mathbf{U}_j$ and $\mathbf{U}_{j+1}$ should be corrected. To this end, after calculating the two solutions by finite difference scheme, say $\mathbf{U}_j^F$ and $\mathbf{U}_{j+1}^F$, we also need to calculate them by cubic interpolations as (2.19), say $\mathbf{U}_j^I$ and $\mathbf{U}_{j+1}^I$. Then at each node, the two solutions are corrected such that only the upwinding information in $\mathbf{U}_j^F$ and $\mathbf{U}_{j+1}^F$ is preserved, giving the following two solutions

$$\mathbf{U}_j = P^- \begin{pmatrix} \mathbf{W}_{j,1}^F \\ \mathbf{W}_{j,2}^I \end{pmatrix}, \quad \mathbf{U}_{j+1} = P^+ \begin{pmatrix} \mathbf{W}_{j+1,1}^I \\ \mathbf{W}_{j+1,2}^F \end{pmatrix},$$

with

$$\mathbf{W}_j^\alpha = (P^-)^{-1}\mathbf{U}_j^\alpha = \begin{pmatrix} \mathbf{W}_{j,1}^\alpha \\ \mathbf{W}_{j,2}^\alpha \end{pmatrix}, \quad \mathbf{W}_{j+1}^\alpha = (P^+)^{-1}\mathbf{U}_{j+1}^\alpha = \begin{pmatrix} \mathbf{W}_{j+1,1}^\alpha \\ \mathbf{W}_{j+1,2}^\alpha \end{pmatrix}$$

representing the partitions of $\mathbf{W}_j^\alpha$ and $\mathbf{W}_{j+1}^\alpha$ based on the signs of the eigenvalues of the coefficient matrix, where $\alpha \in \{F, I\}$.

4 Numerical examples

To test the fourth-order accuracy and the stability of the proposed scheme, several wave systems with available exact solutions are simulated in this section. In all of our numerical examples, the exact solutions are imposed as initial conditions as well as Dirichlet boundary conditions at the boundaries of the computational domains so that we can measure the errors in the numerical solutions and thus investigate the convergence property of the scheme. Also, unless otherwise specified, the exact solutions are utilized in defining jump conditions of the type $[\mathbf{u}] = \mathbf{u}^+ - \mathbf{u}^-$ across material interfaces.

4.1 Linear one-dimensional wave system

We begin by considering the one-dimensional wave system (3.1) in the domain $\Omega = [0, 1]$, with different formulas for the coefficient matrix across the discontinuity $x_d \in (0, 1)$ being

$$A^- = \begin{pmatrix} 0 & 1 \\ 1 & 0 \end{pmatrix} \qquad \text{and} \qquad \mathrm{A}^+ = \begin{pmatrix} 0 & 3 \\ 3 & 0 \end{pmatrix},$$

respectively. One analytical solution $\mathbf{u} = (u_1, u_2)^T$ to this system is

$$u_1(x,t) = \begin{cases} \dfrac{1}{2}\left(\sin(k(x+t)) + \sin(k(x-t)\right), & 0 \le x < x_d, \\ \dfrac{1}{2}\left(\sin(k(x+3t)) + \sin(k(x-3t)\right), & x_d < x \le 1, \end{cases}$$

and

$$u_2(x,t) = \begin{cases} -\dfrac{1}{2}\left(\sin(k(x+t)) - \sin(k(x-t)\right), & 0 \le x < x_d, \\ -\dfrac{1}{2}\left(\sin(k(x+3t)) - \sin(k(x-3t)\right), & x_d < x \le 1, \end{cases}$$

where the wave number k is set as 8π in the following tests, corresponding to a total of four wavelengths in the domain $[0, 1]$.

As mentioned earlier, the overall accuracy of the method is determined by the order of the extrapolation in defining ghost values. To investigate the relationship between the global accuracy of the proposed scheme and the order of the extrapolation, we consider constant, linear, quadratic and cubic extrapolations. For instance, to calculate $\mathbf{U}_{j+1}^G$ and $\mathbf{U}_{j+2}^G$, the following polynomial extrapolant $I(x)$ is employed to define the ghost values, where $P_m(x)$ represents the space of polynomials of degree m or less.

(a) Constant extrapolation: $I(x) = \mathbf{U}^-$.

(b) Linear extrapolation: $I(x) \in P_1(x)$ such that $I(0) = \mathbf{U}_{j-1}$ and $I((1+\theta)\Delta x) = \mathbf{U}^-$.

(c) Quadratic extrapolation: $I(x) \in P_2(x)$ such that $I(-\Delta x) = \mathbf{U}_{j-2}, I(0) = \mathbf{U}_{j-1}$, and $I((1+\theta)\Delta x) = \mathbf{U}^-$. And

(d) Cubic extrapolation: $I(x) \in P_3(x)$ such that $I(-2\Delta x) = \mathbf{U}_{j-3}, I(-\Delta x) = \mathbf{U}_{j-2}, I(0) = \mathbf{U}_{j-1}$, and $I((1+\theta)\Delta x) = \mathbf{U}^-$.

Table 1 shows the error analysis, where $\| E \|$ denotes the relative error in the numerical solution measured in L_∞ norm over all grid points (including the solutions at the interface) at time $t = 10$. For all four cases, we set the interface location at $x_d = 0.5 + \Delta x/2$. Also for this test, the courant number CFL, defined by $\Delta t/\Delta x$, is chosen very small (CFL=0.05) so that the error from time integration is negligible. As can be seen, constant, linear, quadratic and cubic extrapolations are sufficient to guarantee first-, second-, third- and fourth-order global accuracy of the proposed scheme, respectively.

Table 1: Order of accuracy corresponding to constant, linear, quadratic, and cubic extrapolation.

	Constant		Linear		Quadratic		Cubic	
N	$\| E \|$	order	$\| E \|$	order	$\| E \|$	order	$\| E \|$	order
100	1.03E-1		1.59E-2		4.00E-3		3.52E-3	
200	5.05E-2	1.03	4.38E-3	1.86	4.14E-4	3.27	2.01E-4	4.13
400	2.48E-2	1.02	1.11E-3	1.98	4.87E-5	3.09	1.27E-5	3.99
800	1.23E-2	1.01	2.78E-4	2.00	6.18E-6	2.98	7.90E-7	4.01
1600	6.11E-3	1.01	6.93E-5	2.00	7.81E-7	2.98	4.92E-8	4.01
3200	3.05E-3	1.00	1.73E-5	2.00	9.81E-8	2.99	3.07E-9	4.00

We next consider the dependence of CFL on the interface location and the dependence of accuracy on CFL. To this end, we shall test five different cases with the discontinuity x_d at $0.5 + \Delta x/10^8, 0.5 + \Delta x/4, 0.5 + \Delta x/2, 0.5 + 3\Delta x/4$, and $0.5 - \Delta x/10^8$, corresponding to five different cell fractions $\theta = 10^{-8}$, 1/4, 1/2, 3/4, and $1 - 10^{-8}$, respectively. Figure 2 displays maximal errors in L_∞ norm at the time $t = 10$ for two different grid sizes when the CFL numbers range from 0.04 to 0.6. First we have found that, regardless of the interface location, the scheme is stable when CFL$\leq$0.68, and unstable when CFL$\geq$0.69, suggesting that the allowed time step size of the proposed scheme for stability is independent of the interface location. Second, one can see that for this problem the minimal error for the proposed scheme appears to occur at around CFL=0.2, which implies the error in the phase shift being minimal at CFL=0.2. This optimal number might be dependent on the problem, but its independence from the interface location is a favorable and desired feature of the scheme. Another point that can be appreciated

from Fig. 2 (b) is that the numerical approximations are more accurate when the interface is in the middle of a grid cell.

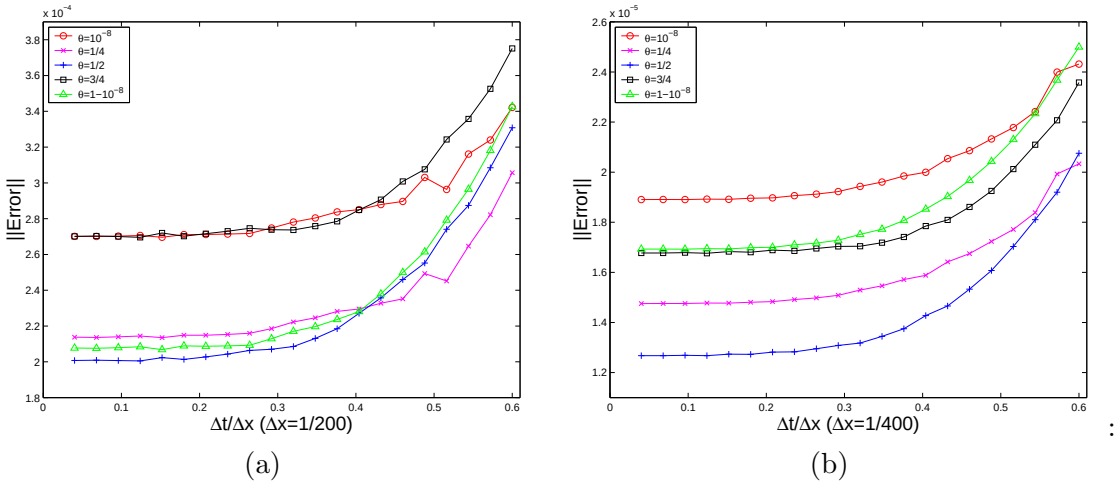

Figure 2: Maximal errors in L_∞ norm versus $\Delta t/\Delta x$ for different cell fraction θ. (a) $\Delta x = 1/200$; (b) $\Delta x = 1/400$. The scheme is stable when CFL$\leq$ 0.68 but becomes unstable when CFL$\geq$ 0.69 (not shown).

We now turn ourselves to the analysis of the convergence rate of the proposed scheme, including its dependence on the interface location. For this reason, we shall again test the above five different cases with the cell fraction θ being $10^{-8}, 1/4, 1/2, 3/4$, and $1-10^{-8}$, respectively. The optimal CFL number (CFL=0.2) is used here, and the relative error $\| E \|$ shown in Table 4.1 is measured at the time $t = 100$ (corresponding to a propagation over a distance of 1200 wavelengths). First, the fourth-order convergence rate of the proposed scheme is clearly observed for all five cases. Second, the numerical results appear to indicate again that, although we obtain the fourth-order convergence rate regardless of the interface location, the numerical approximations are more accurate when the interface is in the middle of a grid cell. In addition, Fig. 3 shows the exact and the numerical solutions at the time $t = 100.55$ for the case of $x_d = 0.5 + \Delta x/2$ with $N = 200$. As being demonstrated, the proposed scheme can correctly capture the interface jump condition.

As pointed out earlier, we employ the classical four-stage Runge-Kutta method as our time-advancing scheme. In general, fourth-order Runge-Kutta schemes can provide relatively large stability regions. For many applications, however, the stability consideration alone is not sufficient, since Runge-Kutta schemes retain both dissipation and dispersion errors. The numerical solutions need to be time accurate to resolve the wave propagation. To examine the long-time stability of our approach, we record and display in Fig. 4 the corresponding errors of the numerical solution as a function of time for the case of $x_d = 0.5 + \Delta x/2$. Note that there is no noticeable growth of the error after running the problem for 100 time units, indicating the scheme will remain stable and fourth-order accurate for long time computations.

Table 2: Grid refinement analysis for the one-dimensional wave system.

	$\theta = 10^{-8}$		$\theta = 1/4$		$\theta = 1/2$		$\theta = 3/4$		$\theta = 1 - 10^{-8}$	
N	$\| E \|$	order	$\| E \|$	order	$\| E \|$	order	$\| E \|$	order	$\| E \|$	order
100	2.99E-3		2.99E-3		3.50E-3		4.73E-3		4.10E-3	
200	2.70E-4	3.47	2.14E-4	3.81	2.04E-4	4.10	2.74E-4	4.11	2.07E-4	4.31
400	1.90E-5	3.83	1.48E-5	3.85	1.28E-5	3.99	1.69E-5	4.02	1.70E-5	3.61
800	1.25E-6	3.93	9.67E-7	3.94	7.96E-7	4.01	1.04E-6	4.02	1.19E-6	3.83
1600	7.96E-8	3.97	6.16E-8	3.97	4.95E-8	4.01	6.45E-8	4.01	7.85E-8	3.92
3200	5.03E-9	3.98	3.89E-9	3.99	3.09E-9	4.00	4.02E-9	4.01	5.03E-9	3.97

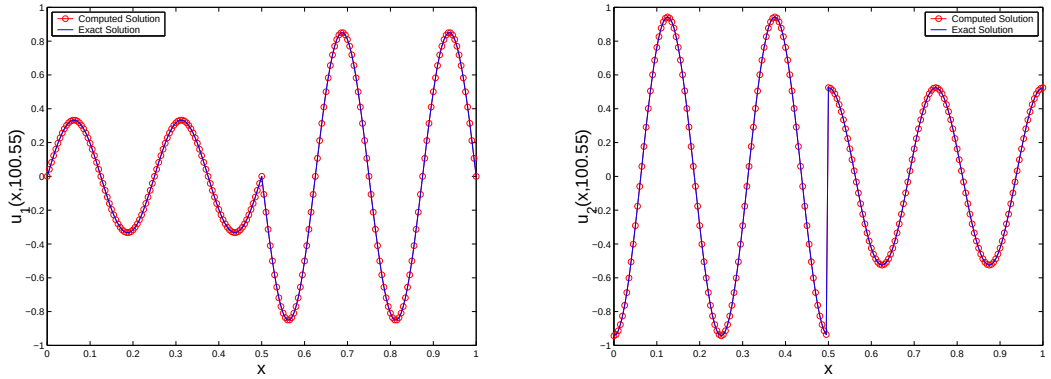

(a) (b)

Figure 3: The exact and the numerical solutions of the one-dimensional wave system at the time $t = 100.55$ for the case of $x_d = 0.5 + \Delta x/2$. (a) $u_1(x, 100.55)$; (b) $u_2(x, 100.55)$.

4.2 One-dimensional Maxwell's equations

As stated earlier, the standard second-order Yee scheme [1] has been widely used in computational electromagnetics. To compare the proposed method with the standard Yee scheme, we shall consider the following one-dimensional Maxwell's equations

$$\epsilon \frac{\partial E}{\partial t} = \frac{\partial H}{\partial z},$$

$$\mu \frac{\partial H}{\partial t} = \frac{\partial E}{\partial z},$$

in the domain $\Omega = [-0.5, 0.5]$ or $\Omega = [-0.5, 0.51]$, where $E(z,t)$ and $H(z,t)$ signify the mutually perpendicular tangential electric and magnetic field components E_y and H_x, respectively, and

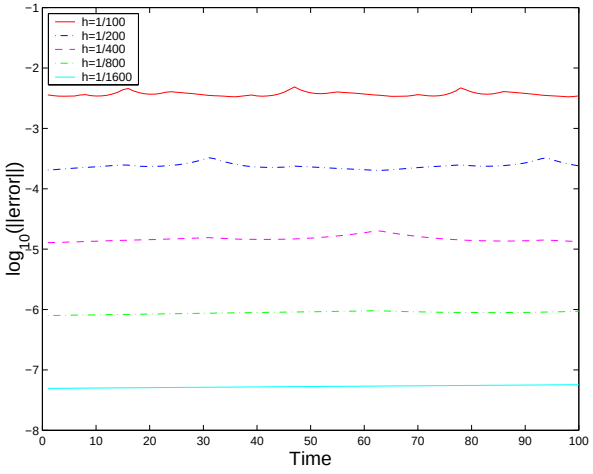

Figure 4: The maximal error in L_∞ norm in the numerical solution as a function of time for the one-dimensional wave system over the time period $[0, 100]$ for the case of $x_d = 0.5 + \Delta x/2$. CFL=0.2 is used in this experiment.

ε and μ represent the material electric permittivity and the material magnetic permeability, respectively.

We take the simple example of a plane wave normally incident on a planar boundary ($z = 0$). On the left of the boundary ($z \leq 0$), the medium is vacuum ($\epsilon_1 = 1, \mu_1 = 1$), but on the right ($0 \leq z$), the medium is a dielectric with $\epsilon_2 = 10$ and $\mu_2 = 2$. When the incident wave encounters the interface between the vacuum and the dielectric, a reflective wave and a transmitted wave will be generated, respectively. To solve the wave propagation problem, the above one-dimensional Maxwell's equations are employed. In our test, the incident plane wave takes the form

$$E_{\text{inc}} = e^{i(\omega t + k_1 z)}, \qquad H_{\text{inc}} = \frac{1}{Z_1} e^{i(\omega t + k_1 z)},$$

where $k_1 = \omega\sqrt{\epsilon_1 \mu_1}$ and $Z_1 = \sqrt{\mu_1/\epsilon_1}$ are the propagation constant and the impedance of the vacuum, respectively. As demonstrated in [32], this problem has an analytical solution given as

follows

$$E(z,t) = \begin{cases} e^{i(\omega t+k_1 z)} + \dfrac{Z_2 - Z_1}{Z_2 + Z_1} e^{i(\omega t - k_1 z)}, & z < 0, \\ \dfrac{2Z_2}{Z_2 + Z_1} e^{i(\omega t + k_2 z)}, & z > 0, \end{cases}$$

$$H(z,t) = \begin{cases} \dfrac{1}{Z_1} e^{i(\omega t+k_1 z)} - \dfrac{Z_2 - Z_1}{Z_1(Z_2 + Z_1)} e^{i(\omega t - k_1 z)}, & z < 0, \\ \dfrac{2}{Z_2 + Z_1} e^{i(\omega t + k_2 z)}, & z > 0, \end{cases}$$

where $k_2 = \omega\sqrt{\epsilon_2\mu_2}$ and $Z_2 = \sqrt{\mu_2/\epsilon_2}$ are the propagation constant and the impedance of the dielectric, respectively. Note that for this case, the solution is actually continuous but not smooth across the interface.

We first solve the above one-dimensional Maxwell's equations in the domain $\Omega = [-0.5, 0.5]$ by the Yee scheme and the proposed scheme with CFL=0.5. Note that the computational domain for this case is symmetric about the interface. So for the following chosen grid sizes, the interface is always on a grid point, i.e., $\theta = 0$ for the proposed scheme. For the Yee scheme, we thus always place the dielectric interface on a magnetic node for the chosen grid sizes, and the permeability μ at this magnetic node is simply taken as the arithmetic average of μ_1 and μ_2. Table 3 shows the results of grid refinement analysis for both schemes, where the relative error $\| E \|$ is measured at the time $t = 100$, clearly indicating the expected second-order convergence rate for the Yee scheme and the expected fourth-order convergence rate for the proposed scheme.

Table 3: Grid refinement analysis for the one-dimensional Maxwell's equations with $\Omega = [-0.5, 0.5]$.

	Yee scheme		UEBM	
N	$\| E \|$	order	$\| E \|$	order
50	2.49E-1		5.93E-2	
100	4.46E-2	2.48	5.89E-3	3.33
200	1.07E-2	2.06	2.92E-4	4.34
400	2.71E-3	1.98	1.56E-5	4.22
800	6.87E-4	1.98	8.96E-7	4.12
1600	1.71E-4	2.01	5.36E-8	4.06
3200	4.28E-5	2.00	3.28E-9	4.03

We then solve the above one-dimensional Maxwell's equations in a slightly different domain

$\Omega = [-0.5, 0.51]$ by the Yee scheme and the proposed scheme with the same number CFL=0.5. Note that the computational domain for this case is not symmetric about the interface. So for the following chosen grid sizes, the interface is not necessarily on a grid point, and for the proposed scheme, the cell fraction θ varies between around 0.01 and 0.75. For the Yee scheme, the same code as in the case of $\Omega = [-0.5, 0.5]$ is used, but now we can no longer guarantee the interface to be placed on either a magnetic or electric node for the chosen grid sizes, but when it happens, the effective dielectric constant at this node is again simply taken as the arithmetic average of the corresponding dielectric constants of the two different media. The relative errors $\| E \|$ measured at the same time $t = 100$ are displayed in Table 4.

As shown in Table 4, the numerical solution obtained by the proposed scheme maintains the fourth-order convergence rate, but that obtained by the standard Yee scheme seems to be only first-order accurate (the average convergence rate is 1) at best, even though for this case the solution is continuous across the interface. Furthermore, the convergence rate of the Yee scheme tends to decrease as the grid size increases, which could be partially understood by the possible localized non-convergent behavior of the scheme, as reported by many authors [3, 4].

Table 4: Grid refinement analysis for the one-dimensional Maxwell's equations with $\Omega = [-0.5, 0.51]$.

	Yee scheme		UEBM		
N	$\| E \|$	order	$\| E \|$	order	θ
50	1.39E-1		8.24E-2		0.7525
100	1.23E-1	0.17	5.33E-3	3.95	0.5050
200	1.16E-2	3.41	3.86E-4	3.79	0.0099
400	5.62E-3	1.04	1.39E-5	4.80	0.0198
800	2.98E-3	0.92	8.00E-7	4.12	0.0396
1600	2.10E-3	0.51	4.76E-8	4.07	0.0792
3200	1.78E-3	0.24	2.84E-9	4.07	0.1584

4.3 A two-dimensional wave problem with material interfaces aligning with coordinate axis

The methodology discussed in Sections 2 and 3 extends naturally to two and three spatial dimensions. For example, in the case of two spatial dimensions, we solve the following two-dimensional z-transverse magnetic (TM) set of Maxwell's equations

$$\frac{\partial \mathbf{u}}{\partial t} + A\frac{\partial \mathbf{u}}{\partial x} + B\frac{\partial \mathbf{u}}{\partial y} = 0, \qquad (x, y) \in \Omega = [a, b] \times [c, d], \tag{4.1}$$

where $\mathbf{u} = (H^x, H^y, E^z)^T$ with E^z and $\mathbf{H} = (H^x, H^y)^T$ representing the scalar electric field and the vector magnetic field, respectively, and

$$\mathbf{A} = \begin{pmatrix} 0 & 0 & 0 \\ 0 & 0 & -1/\mu \\ 0 & -1/\varepsilon & 0 \end{pmatrix}, \quad \mathbf{B} = \begin{pmatrix} 0 & 0 & 1/\mu \\ 0 & 0 & 0 \\ 1/\varepsilon & 0 & 0 \end{pmatrix}.$$

In addition, the solution domain Ω is divided by a dielectric interface Γ into two disjoint pieces, Ω^- and Ω^+, representing two distinct dielectric materials. Across the material interface, the tangential components of the fields should be continuous, yielding the following interface condition

$$\times^+ = \times^-, \ \cdot\mu^{++} = \mathbf{n} \cdot \mu^- \mathbf{H}^-, \ E^{z,+} = E^{z,-}, \tag{4.2}$$

which can be rewritten in a form similar to (3.2), i.e.,

$$R^+ \mathbf{u}^+(\Gamma, t) - R^- \mathbf{u}^-(\Gamma, t) = \mathbf{g}(\Gamma, t), \tag{4.3}$$

with

$$R^\pm = \begin{pmatrix} -n_y & n_x & 0 \\ \mu^\pm n_x & \mu^\pm n_y & 0 \\ 0 & 0 & 1 \end{pmatrix},$$

where $\mathbf{n} = (n_x, n_y)^T$ represents a unit vector normal to the interface Γ.

The spatial derivatives $\mathbf{u}_x$ and $\mathbf{u}_y$ are approximated as

$$(\mathbf{u}_x)_{i,j} \approx \frac{1}{12\Delta x} \left(\mathbf{U}_{i-2,j} - 8\mathbf{U}_{i-1,j} + 8\mathbf{U}_{i+1,j} - \mathbf{U}_{i+2,j} \right), \tag{4.4}$$

$$(\mathbf{u}_y)_{i,j} \approx \frac{1}{12\Delta y} \left(\mathbf{U}_{i,j-2} - 8\mathbf{U}_{i,j-1} + 8\mathbf{U}_{i,j+1} - \mathbf{U}_{i,j+2} \right), \tag{4.5}$$

and for cells cut by the interface Γ, ghost values are defined by extrapolating the value of $\mathbf{u}$ across the interface as described in Section 2. In principle, the definition of the ghost values could be performed in a dimension by dimension fashion, and accordingly, the numerical discretization of $\mathbf{u}_x$ is independent from that of $\mathbf{u}_y$, making the procedure trivial to extend to two and three spatial dimensions. The practical implementation, however, becomes more involved for multi-dimensional cases. One major potential problem is that, for an arbitrary interface and an arbitrary grid, the construction of extrapolants (to define ghost values and calculate interface solutions) in the dimension by dimension fashion may not always be possible for some irregular points due to the limited number of neighboring grid point in a specific direction within the same side of the interface. Generally speaking, when the interface Γ is flat, there shall be enough grid points for us to construct cubic extrapolants to define ghost nodes and calculate interface solutions. For most curved interfaces, however, the dimension by dimension extrapolation may not be applicable. The issue of constructing extrapolants for multi-dimensional problems will be discussed in a forthcoming paper.

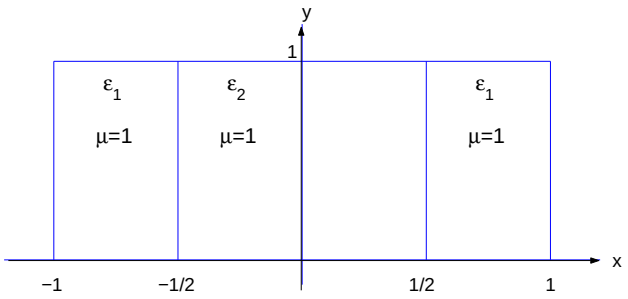

Figure 5: The computational domain of the two-dimensional electromagnetic application.

In this example, we shall investigate the performance of the UEBM for two-dimensional electromagnetic applications where the interfaces are parallel to either the x-axis or the y-axis. The problem being considered here is taken from [6], in which a lossless dielectric with a relative permittivity of ϵ_2 is enclosed by air in x direction, and the media are nonmagnetic and homogeneous along y direction, see Fig. 5. The computational domain $\Omega = \{(x,y)||x| < 1, 0 \leq y \leq 1\}$ is enveloped by PEC walls. An analytical solution for time-varying electromagnetic fields in such a domain is [6]

$$H_x = \begin{cases} -\sqrt{\epsilon_1+3\epsilon_2}\cos\left(\dfrac{2\pi}{3}x\right)\sin(\omega t)\cos(k_y y), & |x| \leq \frac{1}{2}, \quad 0 \leq y \leq 1, \\ -\dfrac{\sqrt{\epsilon_1+3\epsilon_2}}{2}\exp\left(\dfrac{\pi\sqrt{3}}{3}\right)\exp\left(-\dfrac{2\pi\sqrt{3}}{3}|x|\right)\sin(\omega t)\cos(k_y y), & |x| \leq \frac{1}{2}, \quad 0 \leq y \leq 1, \end{cases}$$

$$H_y = \begin{cases} -\sqrt{\epsilon_2-\epsilon_1}\sin\left(\dfrac{2\pi}{3}x\right)\sin(\omega t)\sin(k_y y), & |x| \leq \frac{1}{2}, \quad 0 \leq y \leq 1, \\ -\dfrac{\sqrt{3(\epsilon_2-\epsilon_1)}}{2}\exp\left(\dfrac{\pi\sqrt{3}}{3}\right)\exp\left(-\dfrac{2\pi\sqrt{3}}{3}x\right)\sin(\omega t)\sin(k_y y), & x \geq \frac{1}{2}, \quad 0 \leq y \leq 1, \\ \dfrac{\sqrt{3(\epsilon_2-\epsilon_1)}}{2}\exp\left(\dfrac{\pi\sqrt{3}}{3}\right)\exp\left(\dfrac{2\pi\sqrt{3}}{3}x\right)\sin(\omega t)\sin(k_y y), & x \leq -\frac{1}{2}, \quad 0 \leq y \leq 1, \end{cases}$$

$$E_z = \begin{cases} 2\cos\left(\dfrac{2\pi}{3}x\right)\cos(\omega t)\sin(k_y y), & |x| \leq \frac{1}{2}, \quad 0 \leq y \leq 1, \\ \exp\left(\dfrac{\pi\sqrt{3}}{3}\right)\exp\left(-\dfrac{2\pi\sqrt{3}}{3}|x|\right)\cos(\omega t)\sin(k_y y), & |x| \leq \frac{1}{2}, \quad 0 \leq y \leq 1, \end{cases}$$

where $k_y = \dfrac{2\pi}{3}\sqrt{\dfrac{\epsilon_1+3\epsilon_2}{\epsilon_2-\epsilon_1}}$ and $\omega = \dfrac{4\pi}{3\sqrt{\epsilon_2-\epsilon_1}}$. We will consider the problem herein for $\epsilon_1 = 1$ and $\epsilon_2 = 2, 4$.

Note that for this problem ghost values are needed only for the numerical discretization of $\mathbf{u}_x$, so the scheme reduces to the one-dimensional approach provided only that the jump condition is accounted for correctly based on the upwinding principle [11].

Table 5: Grid refinement analysis for the two-dimensional electromagnetic application.

Grid	$\epsilon_2 = 2$		$\epsilon_2 = 4$	
	$\parallel E \parallel$	order	$\parallel E \parallel$	order
40×40	2.20E-4		2.38E-4	
80×80	1.20E-5	4.20	1.45E-5	4.04
160×160	6.08E-7	4.30	9.57E-7	3.92
320×320	3.26E-8	4.22	6.02E-8	3.99
640×640	1.94E-9	4.07	3.74E-9	4.01
1280×1280	1.16E-10	4.07	2.34E-10	4.00

To verify the fourth-order convergence rate of the proposed scheme, we run this problem for $\epsilon_2 = 2$ and $\epsilon_2 = 4$, respectively, using CFL=0.2 and the mesh size Δx ranging from 1/20 to 1/640. Table 5 indicates the expected fourth-order convergence rate of the proposed scheme on very fine meshes, where the error is measured at the time $t = 1$.

Figure 6 shows the contour and the $y = 0.5$ cross-section of the computed field component H^y at the time $t = 10$ when using a 160×160 mesh for the case of $\epsilon_2 = 4$. Please note that H^y is continuous but its derivative is discontinuous across the material interface. Actually, in this case, it is clear from the interface condition (4.2) that all three field components are continuous across the material interface. The derivative of the E^z component is also continuous across the interface, but the derivatives of the H^x and H^y components are discontinuous.

In Fig. 7, we draw the error in the numerical solution as a function of time over the time period $[0, 10]$ for various grid sizes for the case of $\epsilon_2 = 4$. As being demonstrated, there is no noticeable growth of the error in time.

5 Conclusion

In this paper, using the technique of ghost cells, we have proposed a fourth-order upwinding embedded boundary method for solving one-dimensional time-domain Maxwell's equations with discontinuous coefficients. The proposed scheme retains the simplicity of Cartesian grid based methods while providing the uniformly fourth-order accuracy across the material interfaces at a time step size allowed on the uniform Cartesian mesh. Numerical tests confirm the stability and the global accuracy and ease of implementation of the method.

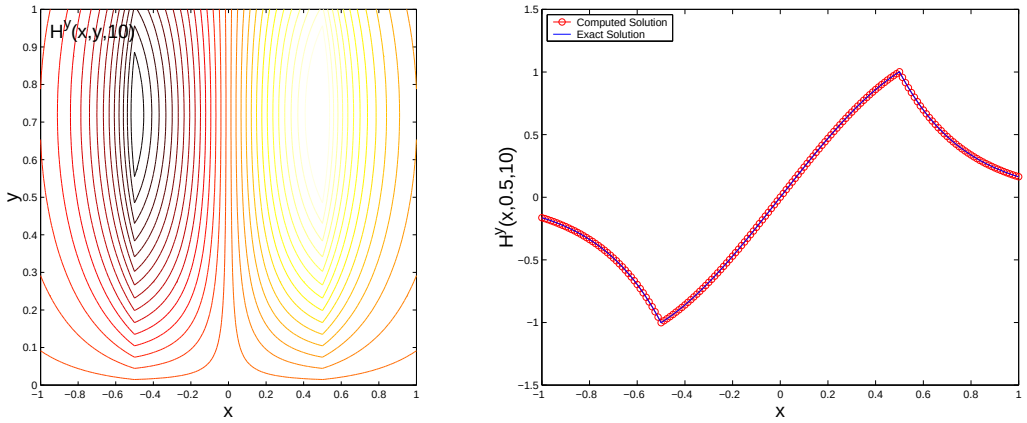

(a) (b)

Figure 6: Electromagnetic field for the two-dimensional electromagnetic application with $\varepsilon_2 = 4$ at $t = 10$. On the left is the contour of the computed field component H^y when using a 160×160 mesh, and on the right is the $y = 0.5$ cross-section of the computed and the exact solutions of the same field component.

Acknowledgments

Wei Cai would like to thank the support of the National Science Foundation (grant numbers: DMS-0408309, CCF-0513179) and the Department of Energy (grant number: DEFG0205ER25678) for the work reported in this paper.

References

[1] K. S. Yee, *Numerical solution of initial boundary value problems involving Maxwell equations in isotropic media*, IEEE Trans. Antennas Propagate. **14** (1966), 302-307.

[2] A. Taflove, Computational Electrodynamics - The Finite Difference Time Domain Method, Artech House, Boston, 1995.

[3] P. Monk and E. Suli, *Error estimates of Yee's method on nonuniform grids*, IEEE Trans. Magn. **30** (1994), 3200-3203.

[4] A. Ditkowski, K. Dridi, and J. S. Hesthaven, *Convergent Cartesian grid methods for Maxwell's equations in complex geometries*, J. Comput. Phys. **170** (2001), 39-80.

[5] T. Xiao and Q. H. Liu, *A staggered upwind embedded boundary method to eliminate the FDTD staircasing error*, IEEE Trans. Antennas Propagat. **52** (2004), 730-741.

[6] A. Yefet and P. G. Petropoulos, *A staggered fourth order accurate explicit finite difference scheme for the time-domain Maxwell's equations*, J. Comput. Phys. **168** (2001), 286-315.

[7] A. Yefet and E. Turkel, *Fourth order compact implicit method for the Maxwell equations with discontinuous coefficients*, Appl. Numer. Math. **33** (2000), 125-134.

[8] Z. Xie, C.-H. Chan, and B. Zhang, *An explicit fourth order staggered finite-difference time-domain method for Maxwell's equations*, J. Comput. Appl. Math. **147** (2002), 75-98.

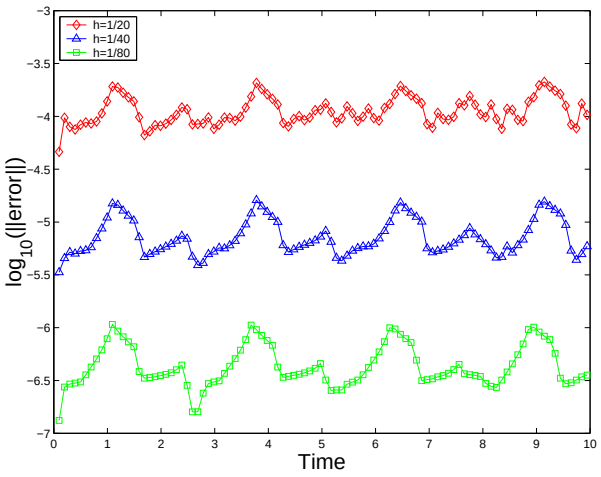

Figure 7: The maximal error in L_∞ norm in the numerical solution as a function of time for the two-dimensional electromagnetic application over the time period $[0, 10]$ for the case of $\epsilon_2 = 4$.

[9] Z. Xie, C.-H. Chan, and B. Zhang, *An explicit fourth order orthogonal curvilinear staggered-grid FDTD method for Maxwell's equations*, J. Comput. Phys. **175** (2002), 739-763.

[10] S. Zhao and G. W. Wei, *High-order FDTD methods via derivative matching for Maxwell's equations with material interfaces*, J. Comput. Phys. **200** (2004), 60-103.

[11] W. Cai and S. Deng, *An upwinding embedded boundary method for Maxwell's equations in media with material interfaces: 2D case*, J. Comput. Phys. **190** (2003), 159-183.

[12] M. J. Berger, C. Helzel, and R. J. LeVeque, *h-box methods for the approximation of hyperbolic conservation laws on irregular grids*, SIAM J. Numer. Anal. **41** (2003), 893-918.

[13] R. B. Pember, J. B. Bell, P. Colella, W. Y. Crutchfield, and M. L. Welcome, *An adaptive Cartesian grid method for unsteady compressible flow in irregular regions*, J. Comput. Phys. **120** (1995), 278-304.

[14] C. Zhang and R. J. LeVeque, *The immersed interface method for acoustic wave equations with discontinuous coefficients*, *Wave Motion* **25** (1997), 237-263.

[15] R. P. Fedkiw, T. Aslam, B. Merriman, and S. Osher, *A non-oscillatory Eulerian approach to interfaces in multimaterial flows (the ghost fluid method)*, J. Comput. Phys. **152** (1999), 457-492.

[16] R. P. Fedkiw, T. Aslam, and S. Xu, *The ghost fluid method for deflagration and detonation discontinuities*, J. Comput. Phys. **154** (1999), 393-427.

[17] X.-D. Liu, R. P. Fedkiw, and M. Kang, *A boundary condition capturing method for Poisson's equation on irregular domains*, J. Comput. Phys. **160** (2000), 151-178.

[18] M. Kang, R. P. Fedkiw, and X.-D. Liu, *A boundary condition capturing method for multiphase incompressible flow*, J. Scientific Comput. **15** (2000), 323-360.

[19] D. Q. Nguyen, R. P. Fedkiw, and M. Kang, *A boundary condition capturing method for incompressible flame discontinuities*, J. Comput. Phys. **172** (2001), 71-98.

[20] F. Gibou, R. P. Fedkiw, L.-T. Cheng, and M. Kang, *A second-order-accurate symmetric discretization of the Poisson equation on irregular domains*, J. Comput. Phys. **176** (2002), 205-227.

[21] F. Gibou and R. P. Fedkiw, *A fourth order accurate discretization for the Laplace and heat equations on arbitrary domains, with applications to the Stefan problem*, J. Comput. Phys. **202** (2005), 577-601.
[22] X. Y. Hu and B. C. Khoo, *An interface interaction method for compressible multifluids*, J. Comput. Phys. **198** (2004), 35-64.
[23] B. Lombard and J. Piraux, *Numerical treatment of two-dimensional interfaces for acoustic and elastic waves*, J. Comput. Phys. **195** (2004), 90-116.
[24] K. Yokoi, F. Xiao, H. Liu, and K. Fukasaku, *Three-dimensional numerical simulation of flows with complex geometries in a regular Cartesian grid and its application to blood flow in cerebral artery with multiple aneurysms*, J. Comput. Phys. **202** (2005), 1-19.
[25] H.-O. Kreiss, N. A. Petersson, and J. Yström, *Difference approximations for the second order wave equation*, SIAM J. Numer. Anal. **40** (2002), 1940-1967.
[26] H.-O. Kreiss and N. A. Petersson, *A second order accurate embedded boundary method for the wave equation with Dirichlet data*, UCRL-JRNL 202686, Lawrence Livermore National Lab, 2004.
[27] H.-O. Kreiss, N. A. Petersson, and J. Yström, *Difference approximations of the Neumann problem for the second order wave equation*, SIAM J. Numer. Anal. **42** (2004), 1292-1323.
[28] H.-O. Kreiss and N. A. Petersson, *An embedded boundary method for the wave equation with discontinuous coefficients*, UCRL-JRNL 215702, Lawrence Livermore National Lab, 2005.
[29] G. Gustafsson, *The convergence rate for difference approximations to mixed initial boundary value problems*, Math. Comp. **29** (1975), 396-406.
[30] G. Gustafsson, *The convergence rate for difference approximations to general mixed initial boundary value problems*, SIAM J. Numer. Anal. **18** (1981), 179-190.
[31] F. Q. Hu, M. Y. Hussaini, and J. L. Manthey, *Low-dissipation and low-dispersion Runge-Kutta schemes for computational acoustics*, J. Comput. Phys. **124** (1996), 177-191.
[32] P. Lorrain, D. Corson, and F. Lorrain, Electromagnetics Fields and Waves, W. H. Freeman and Company, New York, 1988.